e-Blood

MYELOID NEOPLASIA

Multiplexed mAbs: a new strategy in preclinical time-domain imaging of acute myeloid leukemia

Emmet McCormack,[1,2] Maja Mujić,[1] Tereza Osdal,[1,3] Øystein Bruserud,[1,2] and Bjørn Tore Gjertsen[1,2]

[1]Institute of Medicine, Hematology Section, University of Bergen, Bergen, Norway; [2]Department of Internal Medicine, Hematology Section, Haukeland University Hospital, Bergen, Norway; and [3]KinN Therapeutics AS, Haukeland University Hospital, Bergen, Norway

Key Points

- Multiplexing antibodies against common human epitopes all labeled with the same fluorophore facilitates optical imaging of heterogenous AML.
- Multiplexing fluorescently labeled monoclonal antibodies permits optical imaging of primary patient xenograft pathology/therapy response.

Antibodies play a fundamental role in diagnostic immunophenotyping of leukemias and in cell-targeting therapy. However, this versatility is not reflected in imaging diagnostics. In the present study, we labeled anti–human mAbs monochromatically against selected human myeloid markers expressed on acute myeloid leukemia (AML) cells, all with the same near-infrared fluorochrome. In a novel "multiplexing" strategy, we then combined these mAbs to overcome the limiting target-to-background ratio to image multiple xenografts of AML. Time-domain imaging was used to discriminate autofluorescence from the distinct fluorophore-conjugated antibodies. Imaging with multiplexed mAbs demonstrated superior imaging of AML to green fluorescent protein or bioluminescence and permitted evaluation of therapeutic efficacy with the standard combination of anthracycline and cytarabine in primary patient xenografts. Multiplexing mAbs against CD11b and CD11c provided surrogate imaging biomarkers of differentiation therapy in an acute promyelocytic leukemia model treated with all-*trans* retinoic acid combined with the histone-deacetylase inhibitor valproic acid. We present herein an optimizedapplication of multiplexed immunolabeling in vivo for optical imaging of AML cellxenografts that provides reproducible, highly accurate disease staging and monitoring of therapeutic effects. (*Blood*. 2013;121(7):e34-e42)

Introduction

Despite modern advances in therapeutics and improvement in the diagnosis of acute myeloid leukemia (AML) subtypes, the majority of patients die from their disease.[1,2] Thus, in the absence of definitive in vitro models of human AML and failure of significant numbers of new drugs late in clinical trials,[3,4] it is essential that murine AML models are further developed to exploit more specific, targeted therapeutics. Although preclinical development of therapeutics has previously exploited genetic and syngeneic models of AML,[5,6] subcutaneous xenografting of human cell lines in immunodeficient mice has been a popular screening tool.[7] However, the ease of measuring therapeutic efficacy with simple caliper measurements in subcutaneous tumors is offset by the recognition that these models do not typify clinical disease.[8,9] True evaluation of therapeutic potential in this disease necessitates preclinical screening in multiple, systemic, or orthotopic xenograft models of AML, increasingly with primary patient cells that reflect the heterogeneity of the disease.[10]

To facilitate the use of humanized orthotopic AML models in therapeutic settings, investigators have increasingly turned to noninvasive preclinical imaging techniques to define efficacy.[11] Optical imaging of reporter gene expression[12,13] is the preferred modality owing to low cost and high sensitivity. However, the necessity of generating multiple reporter gene–expressing cell lines for drug efficacy studies is both time consuming and expensive, and the potential for additional mutagenic lesions in primary material is a major concern.[14,15] Receptor-targeted imaging probes in which an affinity ligand (eg, a monoclonal antibody [mAb]) to a specific biomarker or epitope is conjugated to a contrast reagent (eg, a near-infrared [NIR] dye) offers an alternative imaging strategy[16] that is exemplified by theranostic imaging of radiolabeled CD45 therapeutic mAb in AML.[17] A drawback of this approach is the difficulty in achieving sufficient target-to-background contrast to completely identify disseminated disease. In particular, determining therapeutic intervention points early in the disease can be difficult to achieve with targeted imaging techniques, primarily due to endogenous autofluorescence and nonspecific fluorescence from exogenous contrast reagents. However, the application of multispectral and, in particular, time-domain optical imaging techniques can at least partially circumvent these issues. Although the use of time-domain optical imaging strategies can enhance signal-to-noise contrast via gating of a fluorophore-specific fluorescence lifetime,[18,19] the expression of sufficient numbers of epitope on target cells is an inescapable constraint for targeted imaging strategies.

We postulated that "multiplexing" multiple mAbs of defined epitopes all labeled with the same fluorophore would increase

Submitted May 19, 2012; accepted November 13, 2012. Prepublished online as *Blood* First Edition paper, December 12, 2012; DOI 10.1182/blood-2012-05-429555.

This article contains a data supplement.

The publication costs of this article were defrayed in part by page charge payment. Therefore, and solely to indicate this fact, this article is hereby marked "advertisement" in accordance with 18 USC section 1734.

fluorescence contrast and provide a set of probes useful in multiple models of AML. In the present study, optimal multiplexing was achieved with 3 mAbs, enhancing contrast 4-fold over single mAbs in in vitro and in vivo phantom studies, with no ill effect on cell viability or proliferation in human AML cell lines and primary AML patient cells. Time-domain imaging of green fluorescent protein (GFP)– or luciferase-expressing AML cell lines with multiplexed mAbs permitted earlier identification of AML xenograft than with either reporter gene. Furthermore, non-reporter gene–expressing human AML cell lines and primary patient xenografts were faithfully imaged with histologic confirmation. Finally, time-domain imaging of multiplexed mAbs was used to demonstrate the therapeutic efficacy of standard chemotherapy and differentiation therapy in AML cell lines and primary patient xenografts.

Methods

Cell lines and primary AML cells

HL-60 (AML French-American-British [FAB] M2), NB4 (AML FAB M3), MOLM-13 (AML FAB 5a), MV4-11 (AML FAB M5) and OCI-AML3 (AML FAB M4) cell lines were purchased from DSMZ. The HL-60, NB4, and MOLM-13 cell lines were cultured in RPMI 1640 medium (Sigma-Aldrich) with 10% FBS, 2mM L-glutamine, and penicillin (50 U/mL)/streptomycin (50 U/mL; both Gibco). The MV4-11 cell line was cultured in IMDM (BioWhittaker, Cambrex Bio Science) with 10% FBS, L-glutamine, and penicillin/streptomycin. OCI-AML3 was maintained in α-MEM with 10% FBS, L-glutamine, and penicillin/streptomycin. AML samples were collected from patients after informed consent in accordance with the Declaration of Helsinki and approval by the local ethics committee (REK Vest, which is affiliated with the University of Bergen and Haukeland University Hospital).

GFP- and luciferase-transduced cells

The $NB4^{GFP}$ [12] and $MOLM\text{-}13^{luc}$ [13] cell lines have been described previously. GFP-expressing cells, including $NB4^{GFP}$ and $HL\text{-}60^{GFP}$, were isolated by cell sorting with a FACSAria cell sorter (BD Biosciences). Luciferase activity in the $MOLM\text{-}13^{luc}$ cell line was measured by adding 1.6 μg/μL of D-luciferin (Promega) to 150 μL of cell suspension (1×10^5 cells/mL) 10 minutes before imaging. The clones with the highest photon intensities were expanded and used for in vivo imaging.

Flow cytometry analysis

In vitro multiplexing studies. A total of 2×10^5 cells were washed and resuspended in 50 μL of 1× PBS. Samples were incubated with 0.4 μg of combinations of 1 (n = 4 combinations), 2 (n = 6 combinations), 3 (n = 4 combinations), and 4 (n = 1 combination) of the following mAbs; CD45-PE (clone MEM-28), CD33-PE (clone HIM3-4), CD13-PE (clone WM15), and HLA ABC-PE (clone W6/32; all Exbio) at room temperature for 30 minutes. Stained cells were washed with 1× PBS and resuspended in 2% paraformaldehyde (Alfa Aesar). All experiments were run in 3 replicates.

Analysis of xenografted BM and blood. CD45-FITC (clone MEM-28; Exbio) or CD33-FITC (clone HIM3-4) and CD34-PE (clone 8G12; both BD Biosciences) were added to 50 μL of mouse blood/bone marrow (BM) and incubated for 30 minutes at 4°C. Lysing buffer (1 mL; Pharm Lyse; BD Biosciences) was added and samples were incubated for another 8 minutes at room temperature and then washed with 1× PBS containing 0.5% BSA. A FACSCalibur (BD Biosciences) was used to perform flow cytometry on 1×10^4 cells for each sample. FlowJo Version 8.8.6 software (TreeStar) was used to analyze flow cytometry data.

Differentiation of all ATRA- and VPA-treated cells. NB4 cells (2×10^5) were treated with 1μM all *trans* retinotic acid (ATRA) (Sigma-Aldrich) and 1mM valproic acid (VPA) (100 mg/mL of Orfiril in solution; Desitin Arzneimittel) for 48 hours. Cells were washed twice with 1× PBS and 50 μL of each sample was incubated with 2.5 μL of CD11b-FITC (clone MEM-174; Exbio), 2.5 μL of CD11c-FITC (clone BU15; Exbio), or both in addition to 0.625 μL of CD33-PE-Cy7 (clone P67.6; BD Biosciences). After 15 minutes, 1× PBS was added and a FACSCanto flow cytometer (BD Biosciences) was used to analyze 1×10^4 live cells.

Conjugation of mouse anti–human mAbs with Alexa Fluor 680

Seven mAbs, including an IgG2a negative control (clone MRC OX-34), CD45 (clone F10-89-4), CD33 (clone WM53), CD13 (clone WM15), HLA ABC (clone W6/32; all AbD Serotec), and CD11b (clone MEM-174) and CD11c (clone BU15; both Exbio), were conjugated to Alexa Fluor 680 using the SAIVI Alexa Fluor 680 Labeling Kit (Invitrogen) as described by the manufacturers. Protein concentrations of the Alexa Fluor 680–conjugated mAbs and degree of labeling was determined with a Nanodrop 1000 spectrophotometer (Thermo Fischer Scientific).

Cell viability and proliferation assays

Evaluation of apoptosis in $NB4^{GFP}$, MOLM-13, HL-60, MV4-11, and OCI-AML3 cells (2×10^4 cells/mL) or 3 primary AML patient cell samples ($2\text{-}5 \times 10^5$ cells/mL) after incubation with Alexa Fluor 680–labeled CD45/13/HLA ABC (4 μg) was performed by DNA-specific staining with Hoechst 33342 (10 μg/mL; Invitrogen),[20] followed by counting of normal and fragmented/condensed cell nuclei using an inverse fluorescence microscope (IRB; Leica Microsystems). To further evaluate if cells were proliferating normally, $NB4^{GFP}$, MOLM-13, HL-60, MV4-11, and OCI-AML3 cells (2×10^4 cells/mL) or 3 primary AML patient cell samples ($2\text{-}5 \times 10^5$ cells/mL) were incubated with CD45/13/HLA ABC (4 μg) and counted after 24 and 48 hours using a Bürker hemocytometer. Viability/proliferation was determined using the Cell Proliferation Reagent WST-1 (Roche Applied Science) according to the manufacturer's protocol. Aliquots (90 μL) of cells (cell lines: 2×10^5 cells/mL, primary AML patient cells: $2\text{-}5 \times 10^5$ cells/mL) incubated with CD45/13/HLA ABC (4 μg) were added to 10 μL of WST-1 24 after the initiation of the experiments. The cells were incubated for 4 more hours and the results were collected using a Tecan Infinite 200 microplate reader and Magellan Version 6 software (Tecan Trading).

Optical imaging

Before imaging, mice were depilated and anesthetized with 1%-2% isoflurane (Isoba; Schering-Plough), 0.2 L/min of O_2, and 0.2 L/min of N_2. NIR images were obtained with the eXplore Optix or Optix MX2 Small Animal Molecular Imager system (ART Inc). NIR imaging scans (λ_{ex} = 670 nm, λ_{em} = 700 LP, laser repetition rate 80 MHz, raster scan points 1 mm apart) were obtained 24 hours after administration of Alexa Fluor 680–labeled mAbs (total mAb concentration of 1 μg/g) as described previously.[19] For GFP fluorescence imaging, an eXplore Optix imager (ART Inc) configured for GFP-imaging experiments (λ_{ex} = 470 nm, λ_{em} = 500 LP, laser repetition rate 40 MHz, raster scan points 1 mm apart) and fluorescence gating of GFP fluorescence lifetime (2.65 ns) was performed as described previously.[12] Optix MX2 (ART Inc) was used for bioluminescence imaging (raster scan points 1 mm apart). Bioluminescent images were performed 10 minutes after the administration of D-luciferin (150 mg/kg). All images and fluorescence lifetime gating were analyzed with Optiview software (Versions 1.04 and 2.02; ART Inc).

Homogenous phantom model

A total of 1×10^6 $NB4^{GFP}$ cells were washed twice with 1× PBS and labeled with 4 μg in total of 1, 2, 3, and 4 Alexa Fluor 680–conjugated mAbs, as described in "In vitro multiplexing studies." Labeled cells were washed twice with 1× PBS and transferred to an optical 96-well reaction plate (MicroAmp; Applied Biosystems). An optical 96-well reaction plate was put in a container with the bottom facing up. Next, 45% agar (Sigma-Aldrich) was added so that the 96-well reaction plate was halfway covered, leaving the encapsulated pellets facing up. After the agar had solidified, the phantom was immersed in a 1% Liposyn and 3% whole blood

solution at different depths as described previously.[12] Imaging was performed using an Optix MX2 imager.

Postmortem mouse model

The fur was removed from a NOD/SCID-β2m^{null} mouse and it was killed by CO_2 inhalation. NB4^{GFP} capsules labeled with 1, 2, 3, and 4 mAbs were implanted subcutaneously, intraperitoneally, intramuscularly, in the kidney, in the brain, and within the thorax as described previously.[12] Laser power and integration time were optimized using the Optiview software and NIR scans were acquired.

Xenograft mouse models

The animal experiments were approved by The Norwegian Animal Research Authority and were performed in accordance with The European Convention for the Protection of Vertebrates Used for Scientific Purposes. NOD/SCID IL2rγ^{null} (NSG) mice (6-8 weeks old; originally a generous gift of Prof Leonard D. Shultz, The Jackson Laboratory) were irradiated with a sublethal dose of 1.5 Gy (60 cGy/min) from a photon radiation source (BCC Dynarray CH4 4 megavolt photon irradiation source) before IV injection. A total of 5-10 × 10^6 NB4^{GFP}, HL-60^{GFP}, MOLM-13^{luc}, MV4-11, OCI-AML3, or patient cells were injected intravenously. mAbs–Alexa Fluor 680 (1 μg/g in total, 0.33 μg/g of each mAb) were injected intravenously 24 hours prior to optical imaging. Alternatively, 5 × 10^6 NB4 cells in a solution of PBS/Matrigel (1:1) were injected subcutaneously in the flanks of NOD/SCID mice (6-8 weeks old; Gades Institute, University of Bergen, Bergen, Norway). Tumors were measured every second day and at 100-150 mm^3, mice were treated orally with 65 mg/kg of ATRA and IP with 350 mg/kg of VPA for 3 days. On day 3, mice were injected with CD11b- and CD11c- Alexa Fluor 680, imaged after 24 hours, and tumors were excised for histology and flow cytometry. Mice injected with AML cells from patient 5 were treated with 500 mg/kg of cytarabine (Ara-C; Sigma-Aldrich) IP for 2 days and 2.5 mg/kg daunorubicin (Sigma-Aldrich) intravenously for 3 days, from day 20-22 after injection of AML cells. Mice were killed following institutional guidelines when moribund as defined by weight loss > 10%, lethargy, and/or hind limb paralysis.

Histology and immunohistochemistry

Infiltrated organs were removed from mice and fixed in 4% paraformaldehyde, followed by routine paraffin embedding. After paraffin embedding, 0.4-μm sections were cut and stained with H&E. Tumors treated with ATRA and VPA were assessed for expression of CD11b (dilution 1:1000, rabbit polyclonal, clone ab75476; Abcam). Images were captured with an Olympus BX51 microscope using 4×, 10×, 20×, and 40× objective lenses. Images were recorded using CellB software (Olympus).

Statistical analysis

Results are presented as means ± SEM. Data were compared using an unpaired, 2-tailed Student *t* test. Correlations were made with the Pearson correlation. Survival data were analyzed using Kaplan-Meier survival analysis and survival distributions were analyzed by the Mantel-Cox log-rank test. Differences greater than $P = .05$ were considered significant. Analyses were performed using Prism Version 5.0 software (GraphPad).

Results

In vitro characterization of the multiplexing strategy

We hypothesized that monochromatically labeled mAbs to common AML antigens would improve the sensitivity of AML detection in vivo. We identified 4 cell-surface epitopes expressed on most AML cell lines and from our patient biobank, and HL-60, NB4, and MOLM-13 AML cells were incubated singly or in cocktails (all possible combinations) of 2, 3, or 4 PE-labeled mAbs of the same total mAb concentration (4 μg) against human-CD13, CD33, CD45, or HLA-ABC epitopes and analyzed by flow cytometry (Figure 1A and supplemental Figure 1A, available on the *Blood* Web site; see the Supplemental Materials link at the top of the online article). Significant increases in mean fluorescence intensity were noted up to 3 mAbs ($P < .01$-$.001$) with no difference noted between 3 or 4 mAbs. NB4^{GFP}, MOLM-13, HL-60, MV4-11, and OCI-AML3 cells (2 × 10^4 cells/mL) or primary AML patient cells cultured ± cocktails of 1, 2, or 3 mAbs over 48 hours in vitro did not demonstrate any differences in apoptosis (supplemental Figure 1B-C), proliferative potential (supplemental Figure 1D-E), or viability/proliferation (WST1, data not shown). To evaluate whether increases in fluorescence would translate into an in vivo setting, the aforementioned antibodies were conjugated with the NIR fluorophore Alexa Fluor 680 with a degree of labeling of 2 fluors/mAb, and concentrated to 1 mg/mL. Pellets of NB4^{GFP} (1 × 10^6) cells[12] were subsequently labeled with 1-4 mAbs (same total concentration; 4 μg), immersed in a 1% liposyn/3% whole blood solution at depths of 1-10 mm, and imaged by time-domain optical imaging (Figure 1B and supplemental Figure 1F). There were no differences in the fluorescence lifetime of the Alexa Fluor 680–conjugated mAbs (1.4 ns) noted between cells incubated with 1-4 mAbs. Similar to the results we acquired from flow cytometry, the combination of 3 mAbs resulted in higher fluorescence than either 1 or 2 mAbs, the significance of which increased with depth ($P < .05$-$.001$), with similar, albeit slightly lower, fluorescence obtained with 4 mAbs. Although the limit of detection for cells incubated with 1 mAb was 5 mm, cells incubated with 2, 3, or 4 mAbs could be distinguished at 7 and 9

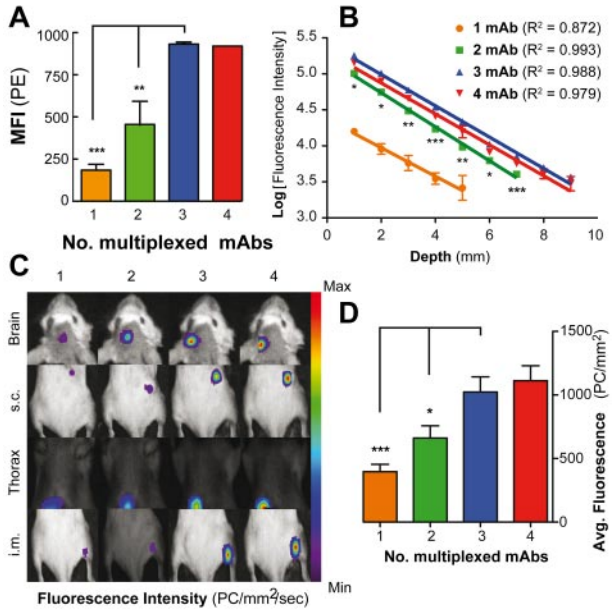

Figure 1. In vitro evaluation of the multiplexing imaging strategy in AML cell lines. (A) Combined flow cytometry results of mAb multiplexing in 3 cell lines (HL-60, NB4, and MOLM-13) using all possible combinations of the mAbs CD33/45/13/HLA ABC as 1 (n = 12), 2 (n = 18), 3 (n = 12), or 4 mAbs (n = 3). Mean fluorescence intensity (MFI) values show means ± SEM. (B) Pellets of 1 × 10^6 NB4^{GFP} cells prestained with 1-4 Alexa Fluor 680–labeled mAbs and immersed into a liposyn solution containing 3% whole blood were imaged at depths of 1-9 mm by time-domain optical imaging. Imaging with 3 multiplexed mAbs results in greater depth detection and increased fluorescence over 1 and 2 mAbs, respectively (mean ± SEM, n = 3). (C) Similarly, cell pellets (1 × 10^6 cells) implanted at defined locations (brain, subcutaneous [s.c.], intramuscular [i.m.], and thorax) in a postmortem mouse illustrates (D) significantly increased fluorescence intensity with increased multiplexing of mAbs (n = 4). Fluorescence images from each panel (eg, brain) have the same scale. *$P < .05$; **$P < .01$; ***$P < .001$.

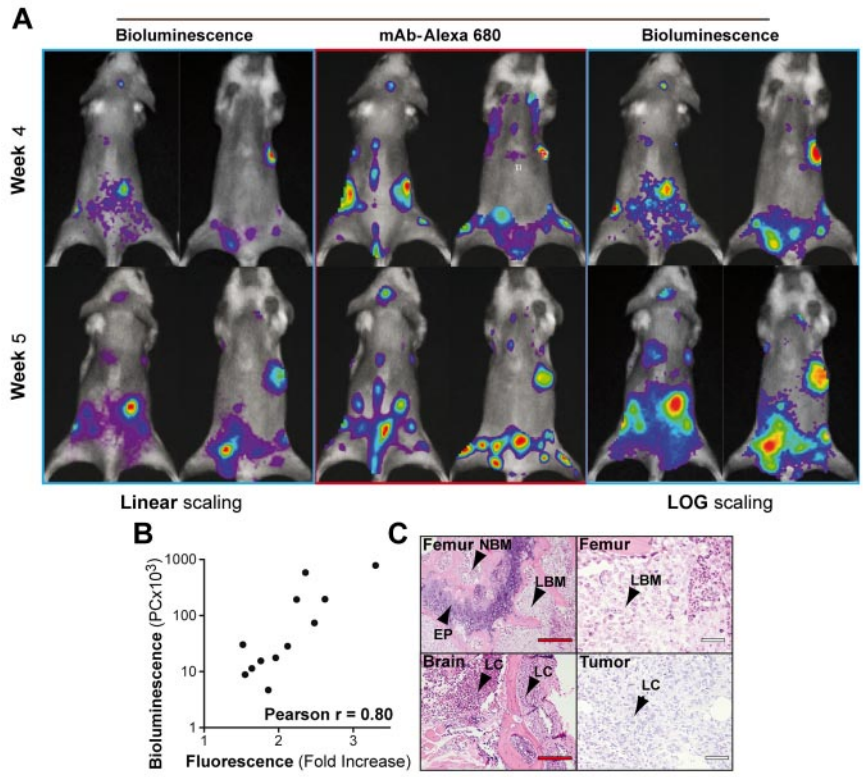

Figure 2. Comparison of multiplexed mAb imaging with bioluminescence. (A) NSG mice (n = 6) previously injected intravenously with 5×10^6 MOLM-13^{luc} cells were imaged for fluorescence and bioluminescence after 4 and 5 weeks. Images were acquired on the same day 24 hours after mAb injection (CD13/45/HLA ABC, total 1 μg/g, 0.33 μg/g of each antibody) and 10 minutes after luciferin administration (150 mg/kg IP). Images depict the maximum to minimum fluorescence/bioluminescence for each mouse. Bioluminescence images on weeks 4 and 5 are shown with both log and linear scaling to permit optimal visualization of leukemic infiltrates. (B) A very good correlation with Pearson correlation coefficient = 0.80 was noted between total bioluminescence and the fold increase in fluorescence. (C) All leukemic infiltrates were confirmed histologically. EP indicates epiphyseal plate; LBM, leukemic bone marrow; LC, leukemic cells; NBM, normal bone marrow; and PC, photon counts.

mm, respectively, with fluorescence detection at depth well correlated (r^2 = 0.89, 0.81, 0.75, and 0.74, respectively). To confirm these results, we implanted the same pellets of NB4^{GFP} cells at different anatomical locations in a postmortum mouse, as described previously,[12] and imaged with time-domain optical imaging. Fluorescence gated images for the fluorescence lifetime of Alexa Fluor 680, described previously,[19,21] again demonstrated superior visualization of cells with increasing mAb number (Figure 1C-D). Quantification of the average fluorescence intensities at all anatomical locations also demonstrated that the use of 3-4 mAbs significantly increased fluorescence output compared with 1 or 2 mAbs (Figure 1D; $P < .05$-$.001$).

In vivo optical imaging with multiplexed mAbs

We selected the NB4^{GFP} (AML FAB M3) and MOLM-13^{luc} (AML FAB 5a) preclinical AML models as these xenografts have been validated previously in vivo for time-domain optical imaging of GFP and bioluminescence, respectively,[12,13] providing a useful comparison for our multiplexing experiment. NSG mice (n = 12) were injected IV with NB4^{GFP} cells (10×10^6) and underwent time-domain optical imaging 24 hours after injection of either isotype control IgG/Alexa Fluor 680 (n = 1) or mAbs; CD45 mAb (n = 3), CD45/HLA-ABC mAbs (n = 3), or CD45/13/HLA-ABC (n = 5) 3 weeks after leukemic cell injection. The total concentration of antibody solution was the same in each combination and was administered at 1 μg/g. Similarly, NSG mice (n = 6) injected with MOLM-13^{luc} cells (5×10^6) underwent time-domain and bioluminescence imaging 24 hours after injection of 3 multiplexed mAbs (CD45/13/HLA-ABC) or 10 minutes after D-luciferin 4 and 5 weeks after leukemic cell injection. Fluorescence lifetime gating of the isotype control resulted in minimal fluorescence, which was subsequently used as the background cutoff.

As expected in the NB4^{GFP} model, we noted GFP fluorescence primarily in the ovaries and lymph nodes with limited femoral fluorescence (supplemental Figure 2A and supplemental Table 1), as described previously.[12] Interestingly, imaging with multiplexed mAbs portrayed a more extensive disease pattern, particularly in infiltrations of the femur and spine. Although mice imaged with 1 mAb generally exhibited more diffuse labeling, mice inoculated with 3 mAbs demonstrated minimal background and cerebral cortex infiltrations. Further comparison of imaged femurs from mAb-inoculated mice (supplemental Figure 2A white squares) revealed increasing fluorescence with increasing numbers of mAbs, although the total mAb concentration and volume were identical. Ultimately, in vivo imaging with 3 mAbs recognized all GFP infiltrates determined by ex vivo imaging (supplemental Figure 2B). Similar results were observed using primary patient material, with at least a 3-fold increase in fluorescence intensity using 3 mAbs compared with 1 mAb ($P < .001$; supplemental Figure 3).

In general, MOLM-13^{luc} mice imaged with multiplexed mAbs and bioluminescence demonstrated similar visualization of disease pathogenesis between the 2 optical imaging modalities (Figure 2A and supplemental Figure 4) with excellent correlation noted (Pearson $r = 0.80$; Figure 2B). However, there were substantial differences in the ability to detect leukemia in the BM. In several cases (as illustrated for mouse 1 and 2 in Figure 2A and supplemental Figure 4), we only detected minimal bioluminescence from femurs and crania of mice regardless of the intensity of scaling used (Figure 2A and supplemental Figure 4), whereas multiplexed mAbs illustrated bright and progressive leukemia. Histology of excised femurs and brains confirmed extensive leukemia at week 5 (Figure 2C). In addition, it was almost impossible to accurately localize leukemic infiltrates, particularly in more diseased mice imaged with bioluminescence. Large superficial tumors generally dominated the resultant images. In contrast, imaging with multiplexed mAbs permitted the detection of intricate lymph node metastasis with good resolution and full

appreciation of BM, spinal, and cerebral infiltrations compared with bioluminescence (eg, Figure 2A mouse 1, week 5).

Multiple AML models imaged with the same multiplexed mAbs

One of the main criteria in performing these experiments was to identify a pool of fluorescently labeled mAbs that could be used in several models of AML. However, it is also critical for drug development studies that these mAbs do not affect the natural progression of AML. Therefore, in addition to the experiments described above with MOLM-13^{luc} and NB4^{GFP}, we xenografted 2 cohorts of NSG mice with the MV4-11 (AML FAB M5), OCI-AML3 (AML FAB M4), and HL-60 (AML FAB M2) human AML cell lines. One cohort was serially imaged with mAbs at the times indicated and maintained for survival analysis, whereas the control group was only monitored for survival. No differences in survival were noted for mice injected with mAbs compared with controls in any of the cell lines tested (supplemental Table 2). mAbs were able to identify infiltrates in the brains and lungs of MV4-11 and in the stomachs (normally obscured by autofluorescence) of OCI-AML3 models, and this was confirmed ex vivo by histology (supplemental Figure 5A). As observed in MOLM-13^{luc} xenografts, fluorescence increased as a marker of disease progression (supplemental Figure 5B).

Preclinical modeling of heterogeneous primary patient material is increasingly used in the development of new therapeutics[22] with limited means to evaluate engraftment or efficacy by noninvasive means. In the present study, we injected NSG (n = 10) mice with 5 primary patient samples of known immunophenotype (supplemental Table 3) and imaged longitudinally with a multiplex of 3 mAbs (CD45/HLA-ABC/CD13 or CD33 depending on patient immunophenotype). In all cases, primary AML disease progression could be determined with time-domain optical imaging and multiplexed mAbs (Figure 3). Patients 1 (Figure 3A,D), 2 (Figure 3B,F), and 5 (see Figure 5), all of whom were relapsed patients who presented with aggressive AML, increasing fluorescence over time, histologically confirmed BM engraftment, and short survival times (Figure 3H) were found. Positive identification of human cells in peripheral blood could only be determined approximately 1-2 weeks before mice being found to be moribund by flow cytometry (eg, supplemental Figure 6), whereas AML engraftment was evident by day 14 with imaging. The only de novo AML sample in the cohort, that from patient 3, demonstrated transient engraftment by optical imaging (Figure 3C,F). No AML cells were observed in flow cytometry or histology of blood, BM, or spleen after necropsy. There was no engraftment of AML cells from patient 4.

Therapeutic efficacy imaged with multiplexed mAbs

The secondary goal of the present study was to evaluate the potential of multiplexed mAbs to image efficacy in a therapeutic setting. To perform these studies, we used a combination of chemotherapy[3] and differentiation therapy,[23] both standards of care in AML therapy. CD11b and CD11c act as biomarkers of differentiation in the therapy of AML.[24] We proposed that multiplexing mAbs against these epitopes would permit imaging of differentiation therapy in vivo. To examine this hypothesis, we first exposed NB4 cells to differentiation therapy (1μM ATRA and 1mM VPA) for 48 hours and measured the increase in differentiation status by flow cytometry (Figure 4A). A significant increase in fluorescence was noted in treated versus control cells using CD11b and CD11c independently ($P < .001$). However, multiplexing CD11b and CD11c significantly increased detection over either mAb alone

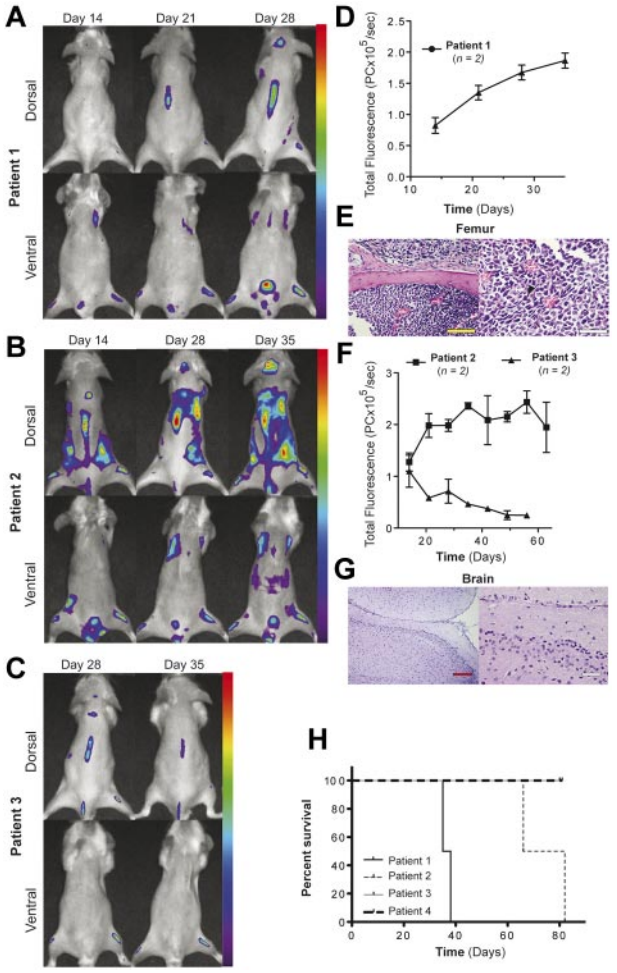

Figure 3. In vivo imaging of primary patient AML xenografts with multiplexed mAbs indicates engraftment status. Four primary AML patient samples (5×10^6 cells) were injected intravenously into irradiated NSG mice (n = 2 per patient sample) and imaged weekly with 3 multiplexed mAbs (CD45/13/HLA ABC, total 1 μg/g, 0.33 μg/g of each antibody). Representative fluorescence images (A-B) and fluorescence quantification (D,F) are shown for patients 1 and 2. All leukemic infiltrates visualized by imaging were confirmed histologically (E,G). Imaging of patient 3 demonstrated transient fluorescence (C), which decreased with time (F), whereas patient 4 (H) did not engraft. In all cases, imaging indicated engraftment success and was confirmed by histology and survival. Scale bars: yellow indicates original magnification of 20×, 0.1 mm; white, original magnification 40×, 0.05 mm.

($P < .01$ and .001, respectively). Subsequently, CD11b and CD11c mAbs were conjugated for in vivo imaging, again with Alexa Fluor 680 as a NIR fluorophore, at a degree of labeling of 2. NSG mice (n = 6) were injected subcutaneously with NB4 cells (5×10^6) and tumors were grown in a volume of 100-150 mm^3. Mice were then treated IP with a combination of ATRA (60 mg/kg) and VPA (350 mg/kg) or vehicle control for 3 days, and tumor volumes were estimated from caliper measurements using the ellipsoidal formula (length × width × height × π/6). On the final day of therapy, all mice were injected with the mAbs CD11b and CD11c, imaged 24 hours later (Figure 4B), and tumors were excised after imaging for ex vivo analysis. Mice receiving therapy demonstrated reduced tumor volumes for the treatment period ($P < .05$ by Student t test; Figure 4D) and significant increases in fluorescence compared with control mice ($P < .05$; Figure 4C), suggesting a differentiation in response to therapy, which was confirmed by immunohistochemistry with CD11b (Figure 4E).

Chemotherapy using a combination of Ara-C and anthracycline (daunorubicin or idarubicin) is the therapeutic mainstay in AML.

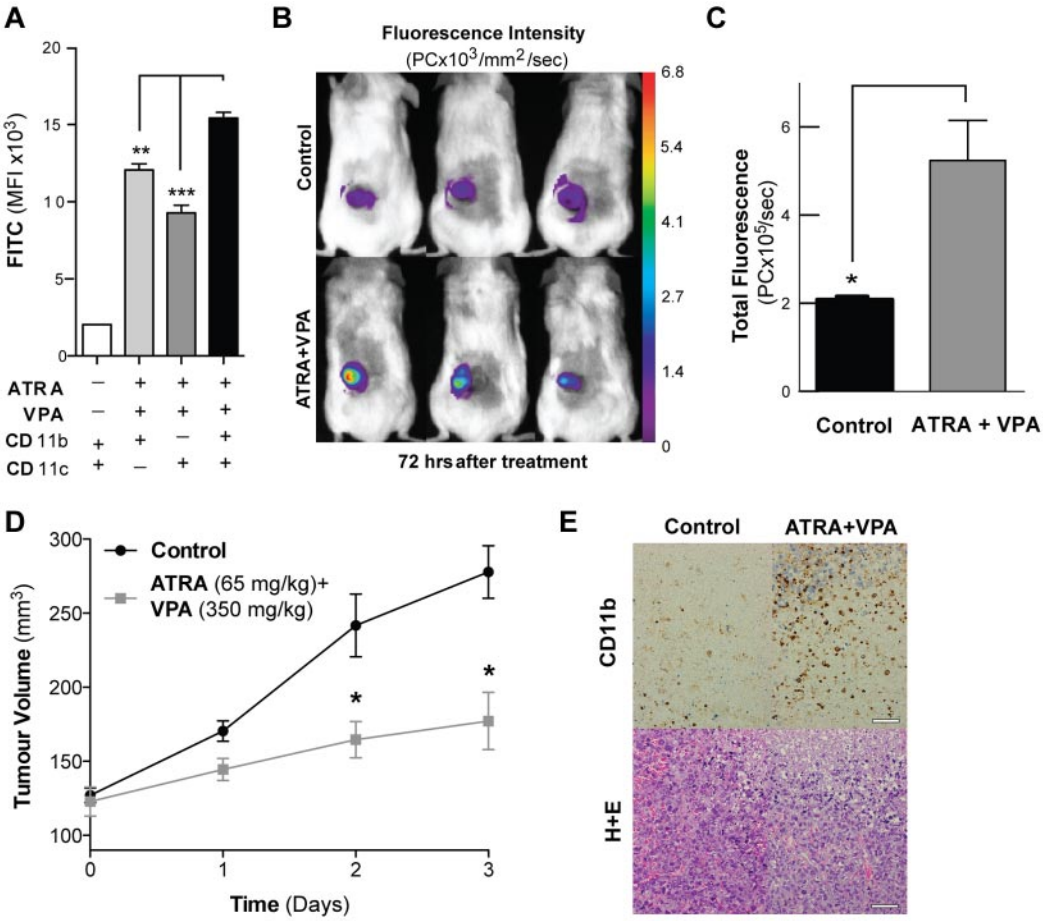

Figure 4. In vivo imaging of differentiation therapy with multiplexed mAbs. (A) Differentiation of NB4 cells treated for 48 hours with a combination of ATRA (1 μM) and VPA (1 mM) as evaluated with CD11b, CD11c or multiplex of both by flow cytometry. Multiplexing of both mAbs provides significant increases in mean fluorescence intensity. $^{**}P < .01$; $^{***}P < .001$. (B) Subcutaneous tumors (n = 4) treated with ATRA (60 mg/kg) and VPA (350 mg/kg) for 3 days show significant increases in fluorescence intensity (C; $^{*}P < .05$) and reduced tumor growth (D; $^{*}P < .05$) compared with controls (means ± SEM, n = 3) and confirmed ex vivo by immunohistochemistry of tumors with CD11b (E). Scale bars: yellow indicates 20×, 0.1 mm; white, 40×, 0.05 mm.

Using 3 multiplexed mAbs, in the present study, we monitored disease development in NSG mice injected with peripheral blood leukocytes harvested from patient 5 (supplemental Table 2). After imaging on day 21 mice were treated with a combination of Ara-C and Daunorubicin or vehicle control and reimaged on day 28 (Figure 5A). After imaging, 50% of mice from both the treated and control groups were killed for ex vivo analysis of BM and spleens; the remaining mice were monitored for survival analysis. Results from imaging with multiplexed mAbs demonstrated a significant difference in disease development 1 week after therapy ($P < .0008$; Figure 5B). Interestingly, although illustrating much lower fluorescence than untreated mice, treated mice still exhibited fluorescence, suggesting residual disease. Flow cytometry analysis of BM from mice killed on day 28 confirmed imaging results, with treated mice demonstrating significantly fewer AML $CD45^+$ ($P < .05$) and $CD34^+$ ($P < .01$) leukocytes and stem cells, respectively (Figure 5C-D). As observed by imaging with multiplexed mAbs, flow cytometry also confirmed the presence of residual disease in the BM (Figure 5D). Survival analysis confirmed therapeutic efficacy in the treated group, with significantly increased survival over controls ($P = .007$), and residual disease, with all mice succumbing to AML by 50 days (Figure 5E). Ultimately, these data sanction the use of multiplexed mAbs as a formidable technique in preclinical imaging of heterogeneous AML disease states and in monitoring therapeutic development.

Discussion

mAbs are unrivalled in their specificity toward defined cellular epitopes and are critical to the success of important clinical techniques such as immunophenotyping[25] and intracellular flow cytometry.[26,27] They are attractive agents for oncologic imaging,[28,29] but several difficulties must be overcome to achieve the necessary specificity and avidity for in vivo contrast.[30] The number of target antigens per cell is a defining factor in the successful application of mAbs for imaging applications.[16] By multiplexing mAbs that were monochromatically labeled with the same fluorophore and targeted toward several antigens expressed on AML cells, we have overcome the limiting contrast to background, as demonstrated with time-domain imaging. This strategy permitted precise disease staging of several preclinical models of AML. We describe here for the first time the utility of this multiplexing strategy to accurately image chemotherapeutic response in primary patient xenografts and direct imaging of tumor differentiation in vivo.

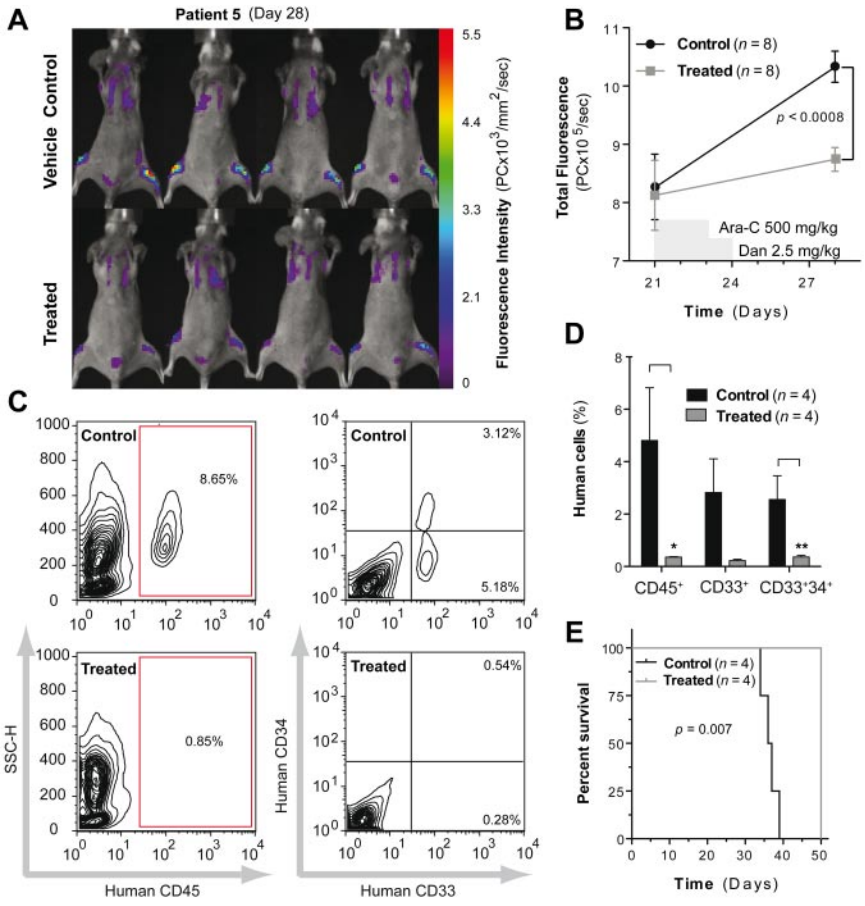

Figure 5. Multiplexed mAb imaging predicts chemotherapy responses in primary patient xenografts of AML. NSG mice (n = 16) injected with AML cells (5×10^6) from patient 5 were treated with Ara-C (500 mg/kg) for 2 days in combination with daunorubicin (2.5 mg/kg) for 3 days. Imaging with multiplexed mAbs was performed before initiation of therapy (day 21) and 1 week later (day 28). (A-B) Representative images of mice after treatment reveal a significant reduction ($P < .0008$) in total fluorescence of treated mice compared with vehicle controls. After imaging on day 28, mice (n = 4 per group) were killed and femoral BM was recovered for flow cytometry analysis of human AML cells (C-D). Significantly reduced human ($CD45^+$; $P < .05$) and leukemic stem cell populations ($CD34^+CD33^+$; $P < .01$) were noted in treated mice. (E) The remaining mice were euthanized when moribund after institutional guidelines; treated mice (n = 4) demonstrated significant increases in survival ($P = .007$) over controls (n = 4).

Numerous monomeric receptor-targeting strategies have been developed to increase tumor contrast over background, including activatable probes,[31] self-quenching moieties,[32] and labeling with multifunctional nanoparticulates.[33,34] Despite limits to the amount of labeling that can be achieved before affecting the specificity, avidity, and pharmacokinetics of the probe in vivo, the number of target antigens per cell is possibly the key restrictive factor. By exploiting the standard immunophenotype of AML patient cells, we selected multiple mAbs of highly expressed epitopes for multiplex detection. Throughout our in vitro and in vivo experiments, contrast saturation was typically achieved at a multiplex of 3 mAbs. Whether this saturation was the result of epitope overload of the cell surface or of fluorophore quenching due to increased proximity is unknown and warrants further investigation. Regardless, contrast enhancement of 3 to 4 fold over single mAbs was demonstrated using 3 multiplexed mAbs, in addition to almost doubling depth detection. Because of the disease heterogeneity, it was difficult to evaluate the multiplexing strategy in vivo using a $NB4^{GFP}$ model, but an increase in the fluorescence with increasing numbers of mAbs was observed in the femur. Using a primary patient xenograft model with a consistent disease pattern, a significantly higher increase in fluorescence intensity was observed in mice imaged with 3 mAbs compared with 1 mAb. The technique was successfully used in imaging several preclinical AML models, including primary patient material. Although we increased the number of mAbs administered to mice, we did not increase the volume or total mAb concentration in an effort to further suppress unspecific background accumulation. Further elaboration of this technique merits optimization of the total protein concentration to be administered in vivo.

In the development of imaging strategies, particularly bona fide exploration of therapeutic efficacy, it is imperative that the contrast reagent itself does not interfere with disease pathogenesis.[35] At no point in the present study did we experience any cellular deviations or changes in model pathogenesis in response to the pool of mAbs used. It was particularly encouraging that this imaging strategy gave better contrast than reporter gene imaging with GFP or bioluminescence in the time-domain configuration and could be used in multiple models of AML and in therapeutic settings. While bioluminescence is generally considered unrivaled in contrast imaging, we demonstrate herein that time-domain imaging of AML with multiplexed mAbs using raster scanning offers superior spatial resolution and appreciation of disease pathogenesis. These results point unequivocally to multiplexed mAbs imaging as the superior paradigm in imaging AML.

Detection and quantification of minimal residual disease is a major issue in monitoring treatment outcomes in AML.[36] In our primary AML xenograft of secondary relapsed disease, residual leukemic infiltrates were evident by imaging 1 week after therapy in accordance with flow cytometry results. Furthermore, the direct effect of a novel combinatorial differentiation therapy could be imaged with multiplexed mAbs against the differentiation biomarkers CD11b and CD11c. To our knowledge, neither primary xenograft therapy monitoring nor biomarker imaging of differentiation have been described previously for AML. Undoubtedly, further validation of this imaging modality's potential will come in

the future through visualization and exploration of novel therapeutics in primary AML xenografts and AML stem cells by multiplexing appropriate antibodies of stem cell markers.

Not only do the results of the present study suggest the potential application of this strategy to other preclinical models of cancer, but also potential clinical translation to extramedullary infiltrations and possibly minimal residual disease detection in AML. There are very few imaging biomarkers approved for clinical use; however, AML imaging with ^{18}F-FLT[37,38] advocates a PET/CT-based multiplexed mAb imaging strategy with appropriate isotopic labeling of humanized mAbs. Such a strategy would necessitate extensive evaluation to determine clinically meaningful benefit over current flow cytometry- and PCR-based techniques. However, with increasing characterization of the leukemic stem cell immunophenotype[39] and advances in novel antibody vectors with improved pharmacokinetics,[16] such a strategy may identify refractory AML earlier.

Acknowledgments

The authors thank M. Popa, L. Vikebø, M. Boge, and K. Jacobsen for expert assistance in all preclinical work; M. Enger for flow cytometry assistance; E. Fick for histology processing; and R. B. Forthun for critical reading of the manuscript. All imaging and flow cytometry sorting were performed at the Molecular Imaging Center, Department of Biomedicine, University of Bergen, Bergen, Norway.

This study was supported by the Norwegian Cancer Society, Western Health Board of Norway, Bergen Research Foundation, and MedViz (www.medviz.uib.no), a medical imaging and visualization research and development cluster in western Norway founded by Haukeland University Hospital, the University of Bergen, and Christian Michelsen Research.

Authorship

Contribution: E.M. optimized the optical imaging methods and orthotopic xenograft models; E.M., M.M., and T.O. performed all of the in vivo studies and analyzed the data; E.M., M.M., and B.T.G. conceived and designed the study and wrote the manuscript; E.M. and B.T.G. provided funding and optical hardware; M.M. and T.O performed all of the in vitro studies; and O.B. isolated and characterized all patient materials.

Conflict-of-interest disclosure: E.M. and B.T.G are shareholders in Kin*N* Therapeutics AS. The remaining authors declare no competing financial interests.

Correspondence: Emmet McCormack, PhD, or Prof Bjørn Tore Gjertsen, MD, PhD, Institute of Medicine, Hematology Section, University of Bergen, Haukeland University Hospital, N-5021 Bergen, Norway; e-mail: emmet.mc.cormack@med.uib.no or bjorn.gjertsen@med.uib.no.

References

1. Rollig C, Bornhauser M, Thiede C, et al. Long-term prognosis of acute myeloid leukemia according to the new genetic risk classification of the European LeukemiaNet recommendations: evaluation of the proposed reporting system. *J Clin Oncol.* 2011;29(20):2758-2765.
2. Pollyea DA, Kohrt HE, Medeiros BC. Acute myeloid leukaemia in the elderly: a review. *Br J Haematol.* 2011;152(5):524-542.
3. Burnett AK. New induction and postinduction strategies in acute myeloid leukemia. *Curr Opin Hematol.* 2012;19(2):76-81.
4. Burnett A, Wetzler M, Lowenberg B. Therapeutic advances in acute myeloid leukemia. *J Clin Oncol.* 2011;29(5):487-494.
5. McCormack E, Bruserud O, Gjertsen BT. Animal models of acute myelogenous leukaemia - development, application and future perspectives. *Leukemia.* 2005;19(5):687-706.
6. McCormack E, Bruserud O, Gjertsen BT. Review: genetic models of acute myeloid leukaemia. *Oncogene.* 2008;27(27):3765-3779.
7. Caponigro G, Sellers WR. Advances in the preclinical testing of cancer therapeutic hypotheses. *Nat Rev Drug Discov.* 2011;10(3):179-187.
8. Kerbel RS. Human tumor xenografts as predictive preclinical models for anticancer drug activity in humans: better than commonly perceived-but they can be improved. *Cancer Biol Ther.* 2003; 2(4 Suppl 1):S134-S139.
9. Peterson JK, Houghton PJ. Integrating pharmacology and in vivo cancer models in preclinical and clinical drug development. *Eur J Cancer.* 2004;40(6):837-844.
10. Pearce DJ, Taussig D, Zibara K, et al. AML engraftment in the NOD/SCID assay reflects the outcome of AML: implications for our understanding of the heterogeneity of AML. *Blood.* 2006; 107(3):1166-1173.
11. Willmann JK, van Bruggen N, Dinkelborg LM, Gambhir SS. Molecular imaging in drug development. *Nat Rev Drug Discov.* 2008;7(7):591-607.
12. McCormack E, Micklem DR, Pindard LE, et al. In vivo optical imaging of acute myeloid leukemia by green fluorescent protein: time-domain autofluorescence decoupling, fluorophore quantification, and localization. *Mol Imaging.* 2007;6(3): 193-204.
13. McCormack E, Haaland I, Venas G, et al. Synergistic induction of p53 mediated apoptosis by valproic acid and nutlin-3 in acute myeloid leukemia. *Leukemia.* 2012;26(5):910-917.
14. Modlich U, Schambach A, Brugman MH, et al. Leukemia induction after a single retroviral vector insertion in Evi1 or Prdm16. *Leukemia.* 2008; 22(8):1519-1528.
15. Baum C. Insertional mutagenesis in gene therapy and stem cell biology. *Curr Opin Hematol.* 2007; 14(4):337-342.
16. Olafsen T, Wu AM. Antibody vectors for imaging. *Semin Nucl Med.* 2010;40(3):167-181.
17. Matthews DC, Appelbaum FR, Eary JF, et al. Development of a marrow transplant regimen for acute leukemia using targeted hematopoietic irradiation delivered by 131I-labeled anti-CD45 antibody, combined with cyclophosphamide and total body irradiation. *Blood.* 1995;85(4):1122-1131.
18. Leblond F, Davis SC, Valdes PA, Pogue BW. Preclinical whole-body fluorescence imaging: Review of instruments, methods and applications. *J Photochem Photobiol B.* 2010;98(1):77-94.
19. Hofmann M, McCormack E, Mujic M, et al. Increased plasma colloid osmotic pressure facilitates the uptake of therapeutic macromolecules in a xenograft tumor model. *Neoplasia.* 2009; 11(8):812-822.
20. Erikstein BS, McCormack E, Tronstad KJ, Schwede F, Berge R, Gjertsen BT. Protein kinase A activators and the pan-PPAR agonist tetradecylthioacetic acid elicit synergistic anti-leukaemic effects in AML through CREB. *Leuk Res.* 2010; 34(1):77-84.
21. Karlsen TV, McCormack E, Mujic M, Tenstad O, Wiig H. Minimally invasive quantification of lymph flow in mice and rats by imaging depot clearance of near-infrared albumin. *Am J Physiol Heart Circ Physiol.* 2012;302(2):H391-401.
22. Saito Y, Kitamura H, Hijikata A, et al. Identification of therapeutic targets for quiescent, chemotherapy-resistant human leukemia stem cells. *Sci Transl Med.* 2010;2(17):17ra9.
23. Bellos F, Mahlknecht U. Valproic acid and all-trans retinoic acid: meta-analysis of a palliative treatment regimen in AML and MDS patients. *Onkologie.* 2008;31(11):629-633.
24. Glasow A, Prodromou N, Xu K, von Lindern M, Zelent A. Retinoids and myelomonocytic growth factors cooperatively activate RARA and induce human myeloid leukemia cell differentiation via MAP kinase pathways. *Blood.* 2005;105(1):341-349.
25. Kern W, Bacher U, Haferlach C, Schnittger S, Haferlach T. The role of multiparameter flow cytometry for disease monitoring in AML. *Best Pract Res Clin Haematol.* 2010;23(3):379-390.
26. Kornblau SM, Minden MD, Rosen DB, et al. Dynamic single-cell network profiles in acute myelogenous leukemia are associated with patient response to standard induction therapy. *Clin Cancer Res.* 2010;16(14):3721-3733.
27. Irish JM, Hovland R, Krutzik PO, et al. Single cell profiling of potentiated phospho-protein networks in cancer cells. *Cell.* 2004;118(2):217-228.
28. Perik PJ, Lub-De Hooge MN, Gietema JA, et al. Indium-111-labeled trastuzumab scintigraphy in patients with human epidermal growth factor receptor 2-positive metastatic breast cancer. *J Clin Oncol.* 2006;24(15):2276-2282.
29. Gmeiner Stopar T, Fettich J, Zver S, et al. 99mTc-labelled rituximab, a new non-Hodgkin's lymphoma imaging agent: first clinical experience. *Nucl Med Commun.* 2008;29(12):1059-1065.
30. Kaur S, Venktaraman G, Jain M, Senapati S,

Garg PK, Batra SK. Recent trends in antibody-based oncologic imaging. *Cancer Lett.* 2012; 315(2):97-111.

31. Tung CH, Mahmood U, Bredow S, Weissleder R. In vivo imaging of proteolytic enzyme activity using a novel molecular reporter. *Cancer Res.* 2000;60(17):4953-4958.
32. Ogawa M, Regino CA, Choyke PL, Kobayashi H. In vivo target-specific activatable near-infrared optical labeling of humanized monoclonal antibodies. *Mol Cancer Ther.* 2009;8(1):232-239.
33. Jung KH, Choe YS, Paik JY, Lee KH. 99mTc-Hydrazinonicotinamide epidermal growth factor-polyethylene glycol-quantum dot imaging allows quantification of breast cancer epidermal growth factor receptor expression and monitors receptor downregulation in response to cetuximab therapy. *J Nucl Med.* 2011;52(9):1457-1464.
34. McCarthy JR, Bhaumik J, Karver MR, Sibel Erdem S, Weissleder R. Targeted nanoagents for the detection of cancers. *Mol Oncol.* 2010;4(6): 511-528.
35. Pesnel S, Pillon A, Creancier L, et al. Optical imaging of disseminated leukemia models in mice with near-infrared probe conjugated to a monoclonal antibody. *PLoS One.* 2012;7(1):e30690.
36. Buccisano F, Maurillo L, Del Principe MI, et al. Prognostic and therapeutic implications of minimal residual disease detection in acute myeloid leukemia. *Blood.* 2012;119(2):332-341.
37. Vanderhoek M, Juckett MB, Perlman SB, Nickles RJ, Jeraj R. Early assessment of treatment response in patients with AML using [(18)F]FLT PET imaging. *Leuk Res.* 2011;35(3): 310-316.
38. Buck AK, Bommer M, Juweid ME, et al. First demonstration of leukemia imaging with the proliferation marker 18F-fluorodeoxythymidine. *J Nucl Med.* 2008;49(11):1756-1762.
39. Buss EC, Ho AD. Leukemia stem cells. *Int J Cancer.* 2011;129(10):2328-2336.